Published in IEEE Trans. On Microwave Theory and Techn,
vol. 62(2), pp. 197-207, 2014.

An analysis of the Leap-Frog Discontinuous Galerkin method for Maxwell's equations

Jesus Alvarez, *Member, IEEE*, Luis D. Angulo, Miguel R. Cabello
A. Rubio Bretones, *Senior Member, IEEE*, and Salvador G. Garcia, *Member, IEEE*

***Abstract*—In this paper, we explore the accuracy limits of a Finite-Element Time-Domain method applied to the Maxwell equations, based on a Discontinuous Galerkin scheme in space, and a Leap-Frog temporal integration. The dispersion and dissipation properties of the method are investigated, as well as the anisotropy of the errors. The results of this novel analysis are represented in a practical and comprehensible manner, useful for the application of the method, and for the understanding of the behavior of the errors in Discontinuous Gelerkin Time-Domain methods. A comparison with the Finite-Difference Time-Domain method, in terms of computational cost, is also included.**

***Index Terms*– Finite-element methods, Discontinuous Galerkin, Time-domain analysis.**

I. INTRODUCTION

Since the FDTD method was firstly proposed by Yee in 1966 [1] for solving Maxwell's equations, it has become undoubtedly the most widespread method among physicists and engineers, due to its simplicity and flexibility to deal with real problems. However, its inability to effectively handle complex geometries, due to stair-casing error, and the limitations in the accuracy (second order in space and time $O\left(h^2, \Delta t^2\right)$), prompted some scientists to search for alternatives long ago, with Finite Element (FE) the obvious alternative. Considering all the schemes based on FE in the literature, Discontinuous Galerkin Time Domain (DGTD) approaches have most of the advantages of FDTD; spatial explicit algorithm, simplicity, easy parallelization, and memory and computational cost growing linearly with the number of elements. Besides, DGTD schemes retain most of the benefits of FE, adaptability of the unstructured meshes and spatial super-convergence, allowing to deal with problems where the required precision varies over the entire domain, or when the solution lacks smoothness.

The performances of the Yee algorithm is very well described in a broad literature [2]. Analytical expressions can be easily derived to analyze the numerical dispersion, stability and anisotropy of the error, due to the use of structured meshes, which enables to find close and general relations. In FETD methods, where unstructured meshes are used, the relations between order of the basis functions (p), element size (h), and time step (Δt) with dispersion, dissipation, and anisotropy, are problem-dependent. The typical approach to analyze the performance of these methods are based on eigenvalue problems [3]–[6] or in solving specific numerical problems [7]. An anisotropic analysis in 2D of the DG TD method for wave propagation problems appears in [8]. Some analyses also include the effect of the time-integration scheme [9].

In this paper, we present an analysis of the accuracy and computational cost of the Leap-Frog Discontinuous Galerkin (LFDG) algorithm, finding practical criteria for its application to general problems. We begin by summarizing the LFDG algorithm. We next analyze the convergence and anisotropy of the algorithm, comparing to the semi-discrete DG space operator. For this, we find the solutions of the eigenvalue problem for a canonical geometry, which can be easily used to also compare to the well-known FDTD method. Finally, a computational cost versus accuracy analysis of the LFDG method is performed and compared to the FDTD method.

The work described in this paper and the research leading to these results has received funding from the European Community's Seventh Framework Programme FP7/2007-2013, under grant agreement no 205294 (HIRF SE project), and from the Spanish National Projects TEC2010-20841-C04-04, CSD2008-00068, and the Junta de Andalucia Project P09-TIC-5327.

The first author is with Cassidian, EADS-CASA, Avda. John Lennon s/n. 28906 Getafe, Spain. The other authors are with the Dept. of Electromagnetism, University of Granada, Fuentenueva s/n, 18071 Granada, Spain, Corresponding author: e-mail: salva@ugr.es, Ph.: +34 958 240507, fax: +34 958 242353.

II. LFDG ALGORITHM

A. Semi-discrete DG formulation

Let us divide the space into M non-overlapping elements V^m, each bounded by ∂V^m, and define element-by-element a set of Q local continuous basis of vector test functions ($\mathcal{B}^m = \{\mathbf{\Phi}_1^m, \mathbf{\Phi}_2^m, ..., \mathbf{\Phi}_Q^m\}$). In this work, vector basis has been used and more specifically, hierarchical high-order vector-basis functions, [10], [11], which present some implementation advantages in order to reduce computation and memory requirements [12]. Now, assume Maxwell's symmetric curl equations for linear isotropic homogeneous media in Cartesian coordinates. Enforcing the residual of Maxwell's curl time-domain (TD) equations to be orthogonal to each basis function element-by-element, we find

$$\left\langle \mathbf{\Phi}_{q'}^m, \varepsilon \partial_t \mathbf{E}^m - \nabla \times \mathbf{H}^m \right\rangle_{V^m} = 0 \tag{1}$$

$$\left\langle \mathbf{\Phi}_{q'}^m, \mu \partial_t \mathbf{H}^m + \nabla \times \mathbf{E}^m \right\rangle_{V^m} = 0 \tag{2}$$

$$\forall q' = (1, \ldots, Q) \ , \ m = (1, \ldots, M)$$

with $\mathbf{E}$, $\mathbf{H}$, ε, μ being, respectively: electric field, magnetic field, permittivity, and permeability. After some algebra, we can write Eqs. (1)(and similarly for Eq. (2)) as

$$\int_{V^m} (\mathbf{\Phi}_{q'}^m \cdot (\varepsilon \partial_t \mathbf{E}^m + \nabla \times \mathbf{\Phi}_{q'}^m \cdot \mathbf{H}^m) dV = \oint_{\partial V^m} \mathbf{\Phi}_{q'}^m \cdot (\hat{\mathbf{n}}^m \times \mathbf{H}^m) dS \tag{3}$$

which relate the volume integral of the LHS to a flux integral in the RHS. DGTD defines continuous numerical fluxes of the tangential field components $\hat{\mathbf{n}}^m \times \mathbf{H}^{m*}$ to be used instead of $\hat{\mathbf{n}}^m \times \mathbf{H}^m$ at the RHS, at each side of ∂V^m. A robust and efficient choice of the numerical flux is the so-called partially penalized flux [13]–[17] which has been proved to provide accurate and free of spurious mode solutions [18],

$$\hat{\mathbf{n}}^m \times \mathbf{H}^{m*} = \hat{\mathbf{n}}^m \times \mathbf{H}^m + \kappa_h^m \left[\hat{\mathbf{n}}^m \times (\mathbf{H}^{m+} - \mathbf{H}^m)\right] - \nu_e^m \left[\hat{\mathbf{n}}^m \times (\hat{\mathbf{n}}^m \times (\mathbf{E}^{m+} - \mathbf{E}^m))\right] \quad (4)$$

with,

$$\kappa_h^m = \frac{Z^{m+}}{Z^m + Z^{m+}},\ \nu_e^m = \frac{\tau}{Z^m + Z^{m+}} \quad (5)$$

τ being a stabilization parameter which penalizes the discontinuities in the tangential components, $Z^m = \sqrt{\frac{\mu^m}{\varepsilon^m}}$ the intrinsic impedance of the element m, and Z^{m+} the intrinsic impedance of the adjacent one. An upwind-flux scheme is obtained with $\tau = 1$, and centered with $\tau = 0$.

Using a Faedo-Galerkin method

$$\mathbf{E}^m = \sum_{q=1}^{Q} e_q^m(t)\mathbf{\Phi}_q^m(\mathbf{r})\ ,\ \mathbf{H}^m = \sum_{q=1}^{Q} h_q^m(t)\mathbf{\Phi}_q^m(\mathbf{r}) \quad (6)$$

a final spatial semi-discrete operator is found

$$\mu\mathbb{M}d_tH^m - \mathbb{F}_{\nu h}H^m + \mathbb{F}^+_{\nu h}H^{m+} = -(\mathbb{S} - \mathbb{F}_{\kappa e})E^m - \mathbb{F}^+_{\kappa e}E^{m+} \quad (7a)$$

$$\varepsilon\mathbb{M}d_tE^m - \mathbb{F}_{\nu e}E^m + \mathbb{F}^+_{\nu e}E^{m+} = (\mathbb{S} - \mathbb{F}_{\kappa h})H^m + \mathbb{F}^+_{\kappa h}H^{m+} \quad (7b)$$

where H^m and E^m are column vectors with the degrees of freedom (dofs), and H^{m+} and E^{m+} the dofs of the adjacent elements, and $\mathbb{M}$ is the mass, $\mathbb{S}$ the stiffness, and $\mathbb{F}$ the flux matrices given in [18].

B. Leap-Frog time integration formulation

For the time integration, we employ the 2^{nd}-order leap-frog (LF) scheme , which is described in the FDTD literature [2]. It samples the unknown fields in a staggered way: the electric field at $t_n = n\Delta t$, and the magnetic field at $t_{n+\frac{1}{2}} = \left(n + \frac{1}{2}\right)\Delta t$. The staggered sampling yields an explicit marching-on-in-time algorithm, assuming that

- The time derivatives in (7) are replaced by 2^{nd}-order accurate central differences[1]

$$\begin{aligned}(d_tH^m)_n &= \frac{H^m_{n+\frac{1}{2}} - H^m_{n-\frac{1}{2}}}{\Delta t} + O\left(\Delta t^2\right)\\ (d_tE^m)_{n+\frac{1}{2}} &= \frac{E^m_{n+1} - E^m_n}{\Delta t} + O\left(\Delta t^2\right)\end{aligned} \quad (8)$$

- The two extra dissipative terms arising from the upwind/penalized flux formulation, are approximated by a backwards formula

$$H_n^m \simeq H^m_{n-\frac{1}{2}}\ ,\ E^m_{n+\frac{1}{2}} \simeq E^m_n \quad (9)$$

Note that if we also employed an average for these terms, a globally implicit scheme would arise (due to the coupling between E and H *DoF* coming from adjacent elements). As discussed in [16], [18] this backward approximation for the flux terms is enough to attenuate spurious modes in space more strongly than physical modes, which is the only aim of these terms.

[1]If there were conductivity terms, these would require a 2^{nd}-order accurate average approximation [19].

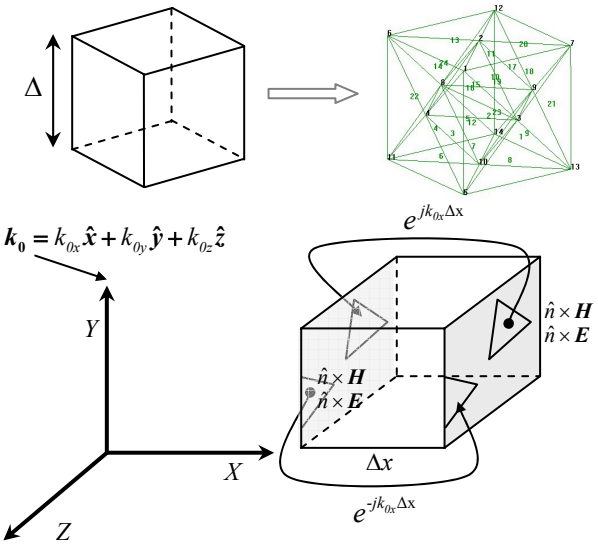

Fig. 1. Geometry under analysis for the eigenvalue problem (top). Application of the PBC between contour faces from elements located at opposite sides.

Inserting the above approximations in (7), we find a fully explicit scheme

$$\begin{aligned}H^m_{n+\frac{1}{2}} =& H^m_{n-\frac{1}{2}} + \frac{\Delta t}{\mu}\mathbb{M}^{-1}\left[-(\mathbb{S} - \mathbb{F}_{\kappa e})E^m_n - \mathbb{F}^+_{\kappa e}E^{m+}_n + \right.\\ & \left.\mathbb{F}_{\nu h}H^m_{n-\frac{1}{2}} - \mathbb{F}^+_{\nu h}H^{m+}_{n-\frac{1}{2}}\right] \quad (10a)\\ E^m_{n+1} =& E^m_n + \frac{\Delta t}{\varepsilon}\mathbb{M}^{-1}\left[(\mathbb{S} - \mathbb{F}_{\kappa h})H^m_{n+\frac{1}{2}} + \mathbb{F}^+_{\kappa h}H^{m+}_{n+\frac{1}{2}} + \right.\\ & \left.\mathbb{F}_{\nu e}E^m_n - \mathbb{F}^+_{\nu e}E^{m+}_n\right] \quad (10b)\end{aligned}$$

III. Description of the eigenvalue problems

In this work, we first formulate the eigenvalue problem for the DG semi-discrete scheme and for the fully discrete LFDG algorithm. Then, we solve this problem for a simple cubic spatial domain in different conditions, in order to study the dispersion and dissipation properties of the schemes, and the anisotropic behavior of the error, as well as being able to directly compare to FDTD.

A. DG semi-discrete scheme

Let us define a column-vector with all the *DoF* of a given problem $\mathbf{U} = \left[\left(h_1^1, ..., h_Q^1\right), ..., ..., \left(e_1^M, ..., e_Q^M\right)\right]^T$. The semi-discrete DG equations (7) (in free-space) can be expressed for plane-wave solutions as the following eigen-problem

$$j\omega\mathbf{U} = \mathcal{A}_{DG}\mathbf{U} \quad (11)$$

with $\mathcal{A}_{DG}$ the semi-discrete DG operator under analysis.

We now consider a cubic spatial domain meshed in a non-symmetrical way into 24 tetrahedrons (Fig. 1), and we

assume that Periodic Boundary Conditions (PBC) conditions are enforced at the box faces by setting

$$\begin{aligned}\hat{\mathbf{n}}^m \times \mathbf{H}^{m+}\big|_{i+\Delta i} &= \hat{\mathbf{n}}^m \times \mathbf{H}^m\big|_i e^{-j\alpha_i},\\ \hat{\mathbf{n}}^m \times \mathbf{E}^{m+}\big|_{i+\Delta i} &= \hat{\mathbf{n}}^m \times \mathbf{E}^m\big|_i e^{-j\alpha_i} \qquad i=\{x,y,z\}\end{aligned} \tag{12}$$

where α_i is the phase shift in each direction of the space here taken as $\alpha_i = k_{0i}\Delta_i$, with $\mathbf{k}_0 = k_{0x}\hat{\mathbf{x}} + k_{0y}\hat{\mathbf{y}} + k_{0z}\hat{\mathbf{z}}$ the analytical wave-vector. We have defined h (a measure for the size of the elements) equal to the dimension of the cube $\Delta \equiv h$.

The eigen-problem (11) is numerically solved for different $\mathbf{k}_0$ to study anisotropy or h for convergence, finding the numerical eigenvalue $\tilde{k}_m$. For the error analysis, we retain only the $\tilde{k}_m$ closest to the analytical one $\mathbf{k}_0 = \omega\sqrt{\mu_0\epsilon_0}$ (the rest can be considered spurious in the sense discussed in [18]), referred to here as $\tilde{k}_0 = \tilde{k}_{real} + j\tilde{k}_{imag}$.

Three different Root Mean Square (RMS) error functions per wavelength ($\lambda = 2\pi/k_0$)) can be defined:

$$\text{RMS error per } \lambda \text{ (dispersion):} \quad \left|e^{-jk_0\lambda} - e^{-j\tilde{k}_{real}\lambda}\right| \tag{13a}$$

$$\text{RMS error per } \lambda \text{ (dissipation):} \quad \left|1 - e^{\tilde{k}_{imag}\lambda}\right| \tag{13b}$$

$$\text{RMS error per } \lambda \text{ (global):} \quad \left|e^{-jk_0\lambda} - e^{-j\tilde{k}_0\lambda}\right| \tag{13c}$$

The first one measures the dispersion error (phase delay), depending on the real part of the numerical eigen-value ($\tilde{k}_{real}$); the second one measures the dissipation error (decrease in amplitude), depending on its imaginary part ($\tilde{k}_{imag}$); and the third one measures the global combination of both errors.

B. Fully discrete LFDG algorithm

In this sub-section, we formulate the fully discrete LFDG scheme (temporal integration plus spatial discretization) eigen-value problem. For this, let us define three column vectors staggered in time

$$\begin{aligned}\mathbf{H}_{n-\frac{1}{2}} &= \left[\left(H^1_{n-\frac{1}{2}}\right)^T, ..., \left(H^M_{n-\frac{1}{2}}\right)^T\right]^T\\ \mathbf{E}_n &= \left[\left(E^1_n\right)^T, ..., \left(E^M_n\right)^T\right]^T\\ \mathbf{U}_n &= \left[\left(\mathbf{H}_{n-\frac{1}{2}}\right)^T, \left(\mathbf{E}_n\right)^T\right]^T\end{aligned}$$

Eqs. (10) (in free-space) can be expressed in a compact manner for the whole spatial domain as

$$\mathbf{H}_{n+\frac{1}{2}} = \left(\mathbb{I}_{MQ} + \frac{\Delta t}{\mu}\mathbb{M}_{\nu h}\right)\mathbf{H}_{n-\frac{1}{2}} + \frac{\Delta t}{\mu}\mathbb{M}_{S\kappa e}\mathbf{E}_n \tag{15a}$$

$$\mathbf{E}_{n+1} = \left(\mathbb{I}_{MQ} + \frac{\Delta t}{\varepsilon}\mathbb{M}_{\nu e}\right)\mathbf{E}_n + \frac{\Delta t}{\varepsilon}\mathbb{M}_{S\kappa h}\mathbf{H}_{n+\frac{1}{2}} \tag{15b}$$

where $\mathbb{I}_{MQ}$ is the $MQ\times MQ$ identity matrix, and $\mathbb{M}_{\nu h}$, $\mathbb{M}_{S\kappa e}$, $\mathbb{M}_{\nu e}$ and $\mathbb{M}_{S\kappa h}$ are $MQ \times MQ$ matrices, which are the result of assembling the element-matrices of (10). Inserting (15a) into (15b), the following fully explicit system is obtained

$$\mathbf{U}_{n+1} = \mathcal{A}_{LFDG}\mathbf{U}_n \tag{16}$$

where the matrix $\mathcal{A}_{LFDG}$ is the Discontinuous Galerkin operator with the Leap-Frog algorithm. It is the result of assembling all the element-matrices of (10) into a $2MQ \times 2MQ$ matrix. The matrix $\mathcal{A}_{LFDG}$ depends on the DG spatial discretization features (mesh size (h), penalization factor (τ), order of the basis functions (p)), and on the time-step (Δt).

Seeking, again, for plane-wave solutions, the relationship between $\mathbf{U}_{n+1}$ and $\mathbf{U}_n$ is

$$\mathbf{U}_{n+1} = e^{j\omega\Delta t}\mathbf{U}_n \tag{17}$$

with $e^{j\omega\Delta t}$ so-called the amplification factor, which is found after solving the following eigen-problem,

$$e^{j\omega\Delta t}\mathbf{U}_n = \mathcal{A}_{LFDG}\mathbf{U}_n \tag{18}$$

Finding the $2MQ$ eigenvalues ($\lambda^m_{\mathcal{A}_{LFDG}}, m = 1, ..., 2MQ$), we obtain the complex-valued numerical wave-vectors ($\tilde{k}^m = \tilde{k}^m_{real} + j\tilde{k}^m_{imag}, m = 1, ..., 2MQ$), related to the eigenvalues by

$$\tilde{k}^m = j\frac{\ln\left(\lambda^m_{\mathcal{A}_{LFDG}}\right)}{c\Delta t}, \qquad m = 1, ..., 2MQ \tag{19}$$

Using the same PBC cubic problem (Fig. 1), and focusing again [18] on the mode closest to the analytical one $\tilde{k}^m = \tilde{k}_0$, we can reproduce the error estimation of Eqs. (13). Notice that $\mathcal{A}_{LFDG}$ is a function of Δt . In the following analyses (except for a specific analysis where we have made Δt variable) , we have fixed this parameter to $\Delta t = 0.7\Delta t_{max}$, with Δt_{max} the upper limit for stability of the LFDG scheme. This is our typical choice to address complex simulations. [13], [18]–[21].

Concerning the evaluation of Δt_{max}, heuristic sufficient stability closed conditions can be found in the literature [12], [16], [22], [23]. However, for the small problem of this paper, we can afford to use a numerical strategy in order to find the least restrictive necessary stability condition case-by-case. For this, we solve the eigenvalue problem (18) for different Δt until we find a maximum value of Δt_{max}, which keeps all the complex-valued $\tilde{k}^m$ with a negative imaginary part ($\tilde{k}^m_{imag} < 0, m = 1, ..., 2MQ$).

IV. Convergence analysis

In this section, we estimate the convergence rates of the semi-discrete DG operator and the fully discrete LFDG algorithm, also studying the influence of the τ penalization parameter, and Δt. The convergence of DG methods has been dealt with in a number of works [3]–[5]. In this paper, we follow the strategy used previously by the authors in [18] for the study of the spurious modes, and the numerical spectrum. We analyze the convergence by searching for numeric plane-wave solutions $e^{j(\omega t - \mathbf{kr})}$ of real frequency ω and complex wave-vector $\mathbf{k}$, for the simple problem of Fig. 1 with PBC, described in the previous section. The numerical wavevector compared to the analytical one will provide a measure for the error of the numerical scheme.

For this analysis, we have taken $\alpha_z = 2\pi\Delta$, and no phase-shift for the other directions $\alpha_x = \alpha_y = 0$ ($\mathbf{k}_0 = k_0\hat{\mathbf{z}}$), since the convergence rates do not depend on the illumination direction. The eigen-problem (11) is numerically solved for different h to find the numerical eigenvalue $\tilde{k}_m$.

For the DG semi-discrete scheme, the RMS for basis orders $p = 1, 2, 3$ and for five values of τ penalization parameter

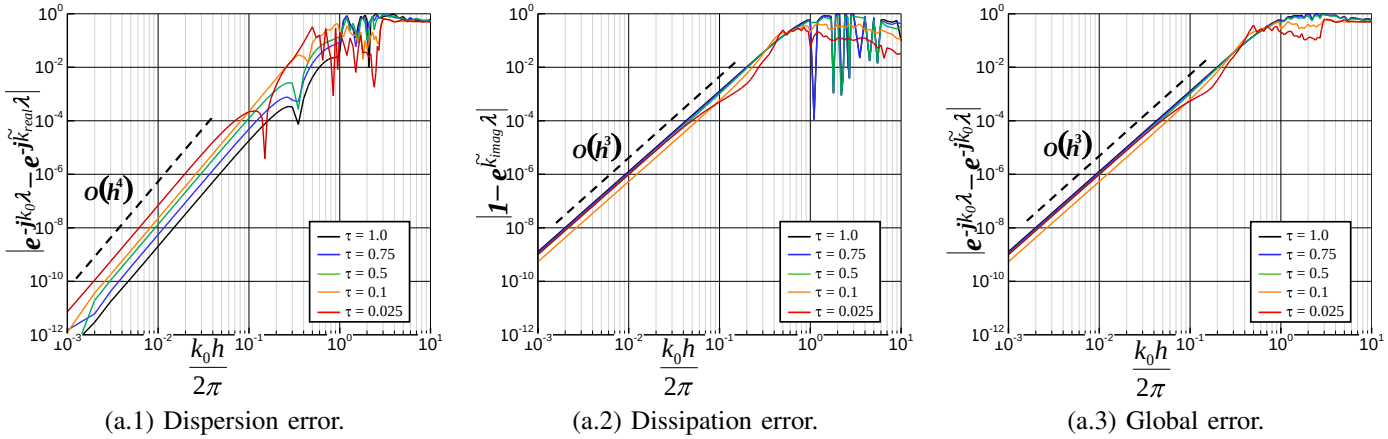

(a.1) Dispersion error. (a.2) Dissipation error. (a.3) Global error.

(b.1) Dispersion error. (b.2) Dissipation error. (b.3) Global error.

(c.1) Dispersion error. (c.2) Dissipation error. (c.3) Global error.

Fig. 2. Convergence and influence of the τ parameter in the error of the DG operator for different p orders. (a) $p = 1$, (b) $p = 2$ and (c) $p = 3$. The dissipation error with a very small value of τ has been computed for $p = 2$ and included in (b.2). In case of $\tau = 0$ (centered flux) the dissipation error would be zero.

(from upwind $\tau = 1$, to $\tau = 0.025$) are shown in Fig. 2 as a function of the spatial resolution ($h/\lambda = k_0 h/(2\pi)$).

From Fig. 2, we can derive the following conclusions:

- Super-convergence of the error is found in all cases. The phase error increases as $O\left(h^{2p+2}\right)$ and the amplitude error follows $O\left(h^{2p+1}\right)$, p being the order of the polynomial space for the vector-basis functions [3]–[5].
- Since the convergence rate for the dissipation error is worse than for the dispersion error ($2p + 2 > 2p + 1$), dissipation places higher constraints on the scheme resolution (h/λ) than does the dispersion error. This fact should be considered when choosing the time integration scheme, to avoid the introduction of more dissipation, keeping dispersion under control. For instance, Runge-Kutta schemes optimize the stability region, while holding dispersion and dissipation fixed. It is found [24] that maximizing dispersion minimizes dissipation, and *vice versa*. LF, as shown below, does not add dissipation error, but only dispersion.
- The parameter τ has little influence in the dispersion and dissipation error of the physical mode, considered here. Only for very low values of τ the dissipation error

decreases, as it should be since $\tau = 0$ (centered) has zero dissipation. Fig. 2(b.2) shows results for a very small value of τ showing this fact. However, it bears noting that the dissipation of the spurious modes is strongly affected by the τ parameter, as demonstrated in [18], and also in the stability condition [16], [17].

Let us now analyze the fully discrete LFDG scheme to compare it with the previous results of the spatial DG operator alone and with the well-known FDTD method. Since the influence of the τ parameter on the accuracy of the physical mode has been seen to be negligible for the semi-discrete case, we have fixed a value of $\tau = 0.1$. This value has been chosen as a trade-off between stability and spurious-mode reduction [18].

Results for RMS errors are shown in Fig. 3 for different orders p, taking $\Delta t = 0.7\Delta t_{max}$. Fig. 4 also shows results for different $\Delta t < \Delta t_{max}$ (for $p = 2$).

We can conclude from Figs. 3 and 4:

- The super-convergence property of the DG spatial operator is maintained up to an error limit where the convergence of the error becomes $O\left(h^2\right)$ dominated by the LF time integration scheme (only 2^{nd}-order). This fact depends neither on the order of functions p, nor on Δt, and coincides with that found for the FDTD method. Higher order Leap-Frog (LF_N) schemes have been proposed to improve this [25].
- Since LF is non-dissipative, only the dispersion error is affected. The dissipation error coincides with that of the semi-discrete case.
- The limit between the zones where the error is dominated by the spatial discretization and by the temporal integration methods depends on Δt, as shown in Fig. 4. This limit can be improved by reducing Δt, at the cost of increasing the computational cost.
- The typical 10^{-2} accuracy value is in the zone dominated by the spatial discretization error for the LFDG method, for $p = 1$, $p = 2$ and $p = 3$ and $\Delta t = 0.7\Delta t_{max}$ with resolutions ranging from $\sim \frac{\lambda}{4.5}$, $\sim \frac{\lambda}{1.9}$ and $\sim \frac{\lambda}{1.1}$, respectively. This characteristic is not expected to be fulfilled by higher orders than $p=3$. In FDTD a resolution of $\sim \frac{\lambda}{28.5}$ can be found from its dispersion relationship [2] to be required to reach a 10^{-2} accuracy[2] for propagation along the cube edge[3] .

A simple numerical experiment has been performed in order to reproduce some results from the previous analysis. A region of $(0.6 \times 0.6 \times 12)$ m. has been meshed into $(3 \times 3 \times 60)$ cubes, each one equal to that used for the previous eigenvalue analysis (Fig. 1, with $\Delta = 0.2$ m.). A y-polarized plane wave, propagating along the z-axis, has been excited at the lower z-plane by using perfect electric conductor (PEC) at

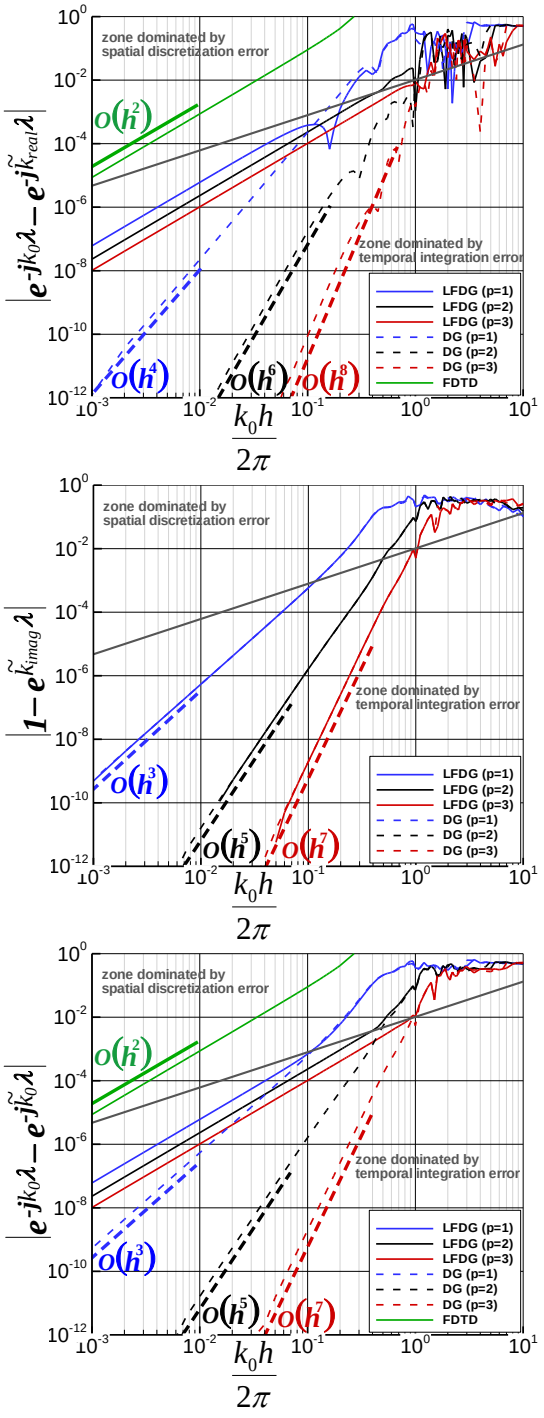

Fig. 3. Convergence of the dispersion (upper), dissipation (middle) and global (lower) errors of the physical mode for the LFDG algorithm with $\tau = 0.1$ and $\Delta t = 0.7\Delta t_{max}$. Analogous curves for the DG operator and FDTD [2] have been included for comparison ($\tilde{k}_0 = \frac{2}{h}\arcsin\left(\frac{h}{c\,\Delta t}\sin(\frac{k_0\,c\,\Delta t}{2})\right)$, $\Delta t_{max} = \frac{h}{c\sqrt{3}}$). In the case of the dissipation error, FDTD curve has been omitted, since the error is zero, and notice that the LFDG and DG curves are superposed. A limit (grey line) has been included in the graphs to separate two zones, one (upper) dominated by the spatial discretization and other (lower) by the temporal integration.

[2]Notice that the resolution for FDTD, is that of the cubic spatial domain of Fig. 1, meshed with one cell, while for LFDG, the same domain is meshed into 24 tetrahedrons. The influence of the resolution is taken into account in Section VI to compare in terms of computational cost.

[3]Propagation along the Cartesian axes is the worst-case of dispersion in FDTD (no phase error occurs along the diagonals at the stability limit). However in a real problem, no control over the propagation direction exists, and a resolution of 28.5 cells/wavelength is reasonable in many FDTD situations.

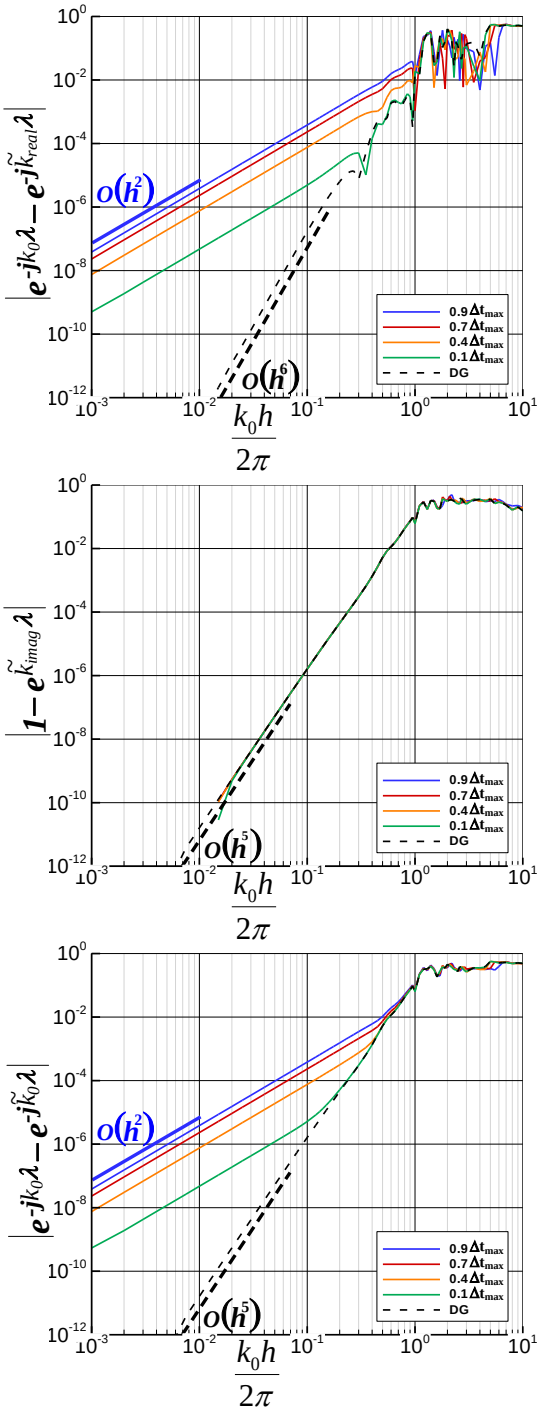

Fig. 4. Influence of Δt in the dispersion (upper), dissipation (middle) and global (lower) errors of the LFDG algorithm with $\tau = 0.1$ and $p = 2$. Analogous curves for the DG operator have been included.

the y-boundaries and perfect magnetic conductor (PMC) at the x-boundaries (which support the plane wave propagation). Silver-Müller absorbing (impedance) boundary conditions [20] have been taken at the z-boundaries.

Two probes separated by $L = 10$ m. along z have been taken to estimate the error in the propagation of the y-component of the electric field $(e_0(t), e_L(t))$. The RMS dissipation error per wavelength has been computed in the frequency domain $(E_0(f), E_L(f))$ by

$$\left| 1 - \left[\frac{|E_L(f)|}{|E_0(f)|} \right]^{\frac{\lambda}{L}} \right| \tag{20}$$

where we have taken into account the multiplicative effect along the propagation path in order to express it in terms of a per-wavelength error and compare to Eq. (13b). For the RMS dispersion error per wavelength, we have computed the numerical phase error with respect to the analytical phase $\left(-\frac{2\pi L}{\lambda}\right)$ and normalized by the wavelengths traveled by the wave $\left(\frac{L}{\lambda}\right)$ to compare with Eq. (13a). Fig. 5 shows this comparison for two different Δt. A good agreement is found for errors above 10^{-7}. Errors below this level happen at very low frequency and are due to truncation of the signals and the presence of spurious modes (a further study of these has been performed in [18]),

V. Anisotropy Analysis

In this section, we analyze the 3D anisotropic behavior of the errors for the semi-discrete DG operator and for the fully discrete LFDG algorithm in 3D (a 2D analysis for the wave propagation problem appears in [8]). In this case, we follow the same strategy used for the convergence analysis. Again, we take $\tau = 0.1$ and $\Delta t = 0.7\Delta t_{max}$ for LFDG. The anisotropic behavior of the error is analyzed by solving the eigenvalue problems for different $\mathbf{k}_0$.

Figs. 6 and 7 show 2D plots of the anisotropic errors for different illumination angles (due to the symmetry of problems $\theta = [0°, 90°]$ and $\phi = [0°, 90°]$ include all the possible illuminations), and basis orders $p = 1, 2, 3$, respectively. 3D representations of the normalized real part of the numerical eigen-value $\left(e^{-j(\tilde{k}_{real} - k_0)\lambda}\right)$ referred to as dispersion rate, and dissipation rates $\left(e^{\tilde{k}_{imag}\lambda}\right)$ have been included to show the shape of the anisotropy[4]. Fig. 8 also shows cuts along the θ angle of the dispersion error for $\phi = 45°$, comparing the DG operator and the LFDG algorithm for different orders p.

From this analysis, we can derive the following conclusions:

- The anisotropy of the error, both dispersive and dissipative, is given by the spatial discretization. The LF temporal integration only introduces an offset in the dispersion error in all directions, and no dissipation error (as expected).
- For conciseness, plots for different values of h and p have been omitted, but we have observed, in general, that

[4]Notice that the rate magnitudes, represented in the 3D figures, gives different information than the 2D plots. The rates are accumulative factors per wavelength, having the dispersion rate information of the phase error sign, which changes if the numerical phase speed is larger or smaller than the analytical one.

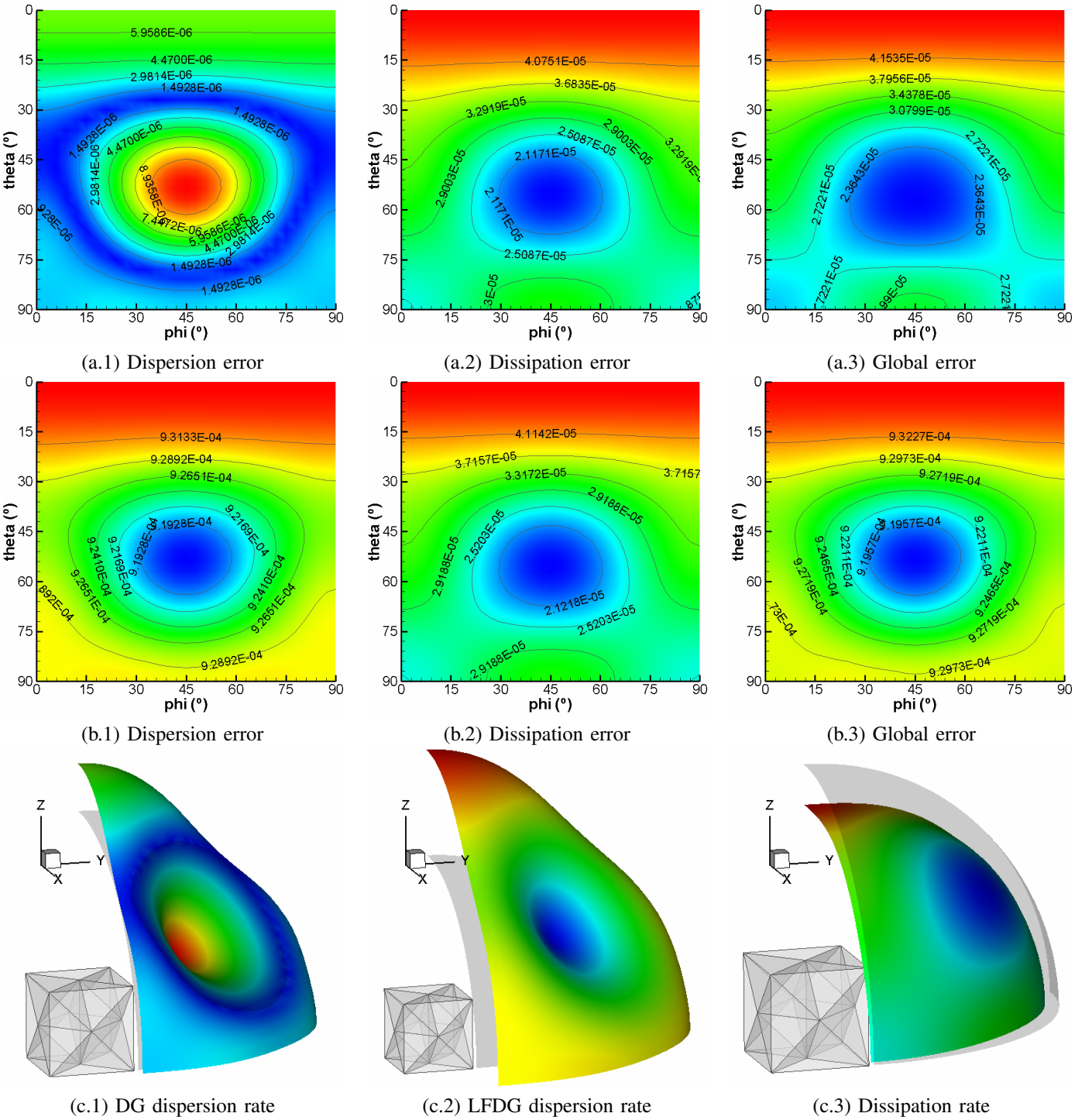

(a.1) Dispersion error (a.2) Dissipation error (a.3) Global error

(b.1) Dispersion error (b.2) Dissipation error (b.3) Global error

(c.1) DG dispersion rate (c.2) LFDG dispersion rate (c.3) Dissipation rate

Fig. 6. Anisotropy of the error for $\tau = 0.1$, $p = 2$ and $h = 0.2$. (a) DG semi-discrete scheme, (b) LFDG scheme with $\Delta t = 0.7\Delta t_{max}$ (c) 3D representation. The error has been amplified in order to represent the shape of the anisotropy. The analytical solution has been represented in grey (sphere of radio 1).

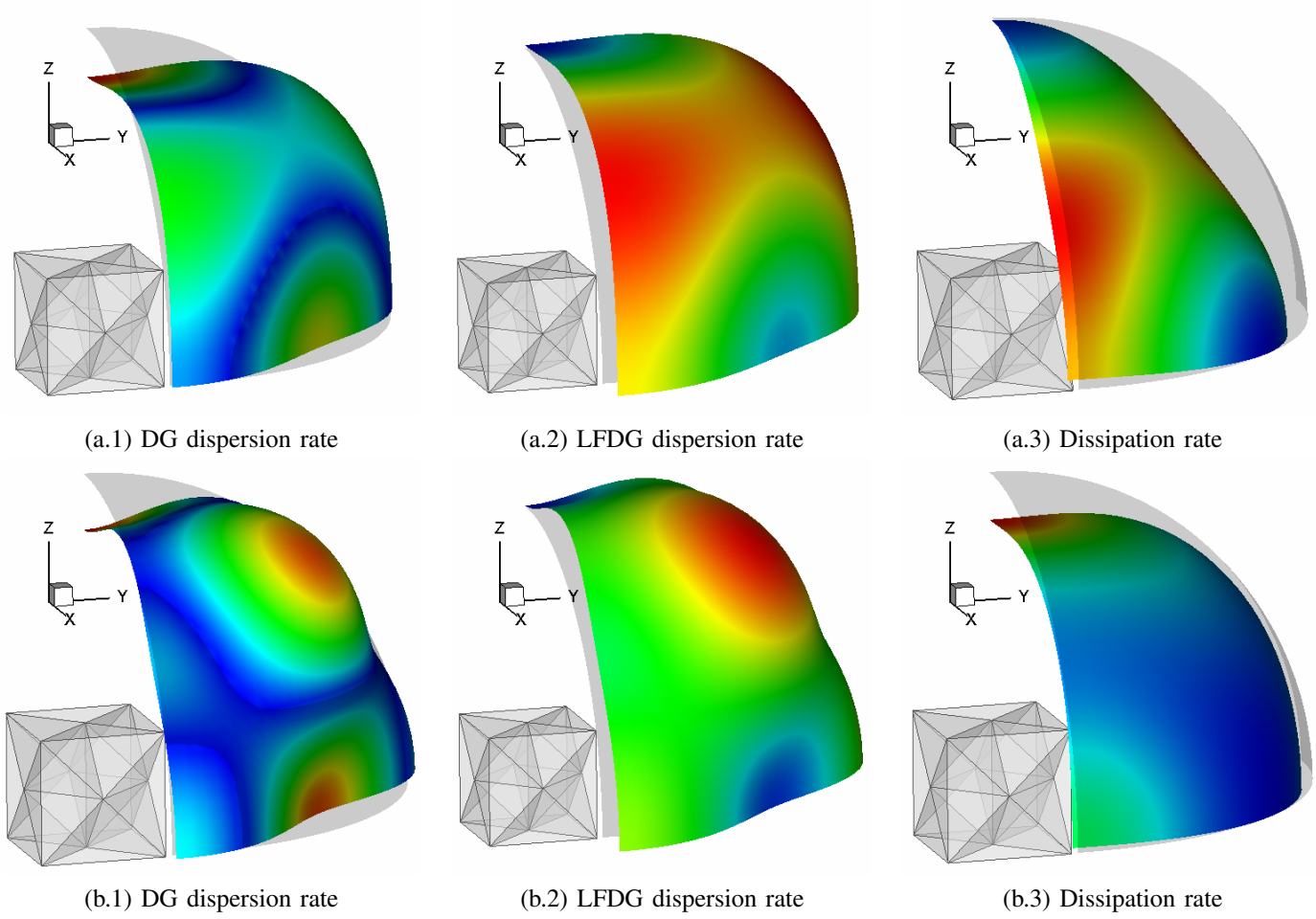

(a.1) DG dispersion rate (a.2) LFDG dispersion rate (a.3) Dissipation rate

(b.1) DG dispersion rate (b.2) LFDG dispersion rate (b.3) Dissipation rate

Fig. 7. 3D representations of the anisotropy of the error for $\tau = 0.1$, $h = 0.25$, (a) $p = 1$ and (b) $p = 3$. The error has been amplified in order to represent the shape of the anisotropy. The analytical solution has been represented in grey (sphere of radio 1).

the shape of the anisotropy of the error (both dispersive and dissipative) only depends on the order of the basis functions (p), while the h-parameter mainly affects to the error amplitude.

- For the semi-discrete DG operator the numerical phase speed is higher than 1.0 for some directions, and lower for some others. That implies that the semi-discrete DG operator has dispersion-free propagation directions.

VI. Computational cost vs. accuracy

The differences in accuracy between LFDG and FDTD (apparently high from Fig. 3) should be analyzed with both methods under fair comparison conditions. In this section, we study the computational cost vs. accuracy in order to draw an effective application of the proposed scheme in real problems and explore the limitations and the efficiency of the method. The main trade-off involves the order of the basis functions p, the mesh resolution h, and accuracy, with the aim of minimizing the computational cost. We must take into account that:

- Increasing p improves accuracy but requires shorter Δt for stability, and the computational cost per element is higher.
- Decreasing h improves accuracy but requires shorter Δt for stability for smaller elements, and the number of elements increases.

To compare the different configurations of the method, a computational cost per λ^3 and picosecond (psec) has been defined. The computational cost for one element of a DG scheme is proportional to the square of the number of basis functions Q in that element

$$C_{element} \propto Q^2 \tag{21}$$

The cost for one time step per λ^3, will be approximately the number of elements M per λ^3 multiplied by the cost per element,

$$\frac{C_{\text{time step}}}{\lambda^3} \approx \frac{M}{\lambda^3} C_{element} \tag{22}$$

Finally, we can define the following figure of merit (CC) to measure the global cost of the method, also including the effect of the Δt taken for stability

$$CC = K \frac{M}{\lambda^3} Q^2 \frac{1}{\Delta t(\text{in psec.})} \tag{23}$$

with K being a factor that has been considered equal to 1 for the FDTD case, and equal to 2 for the LFDG method

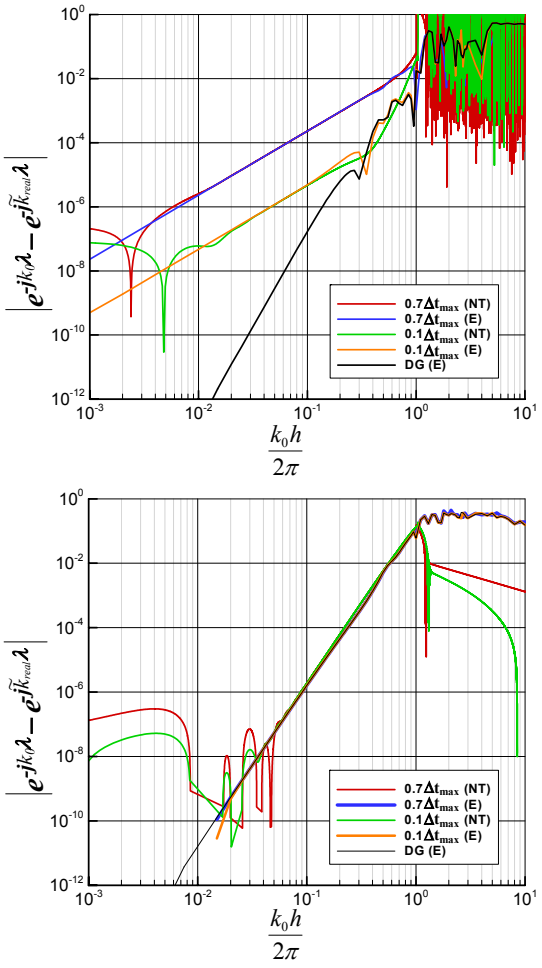

Fig. 5. Convergence of the dispersion (up) and dissipation (down) errors of the LFDG algorithm computed with the numerical test (NT) and with the eigenvalue analysis (E). We have used in both cases $\tau = 0.1$, and $p = 2$. Analogous curves for the DG operator have been included for comparison.

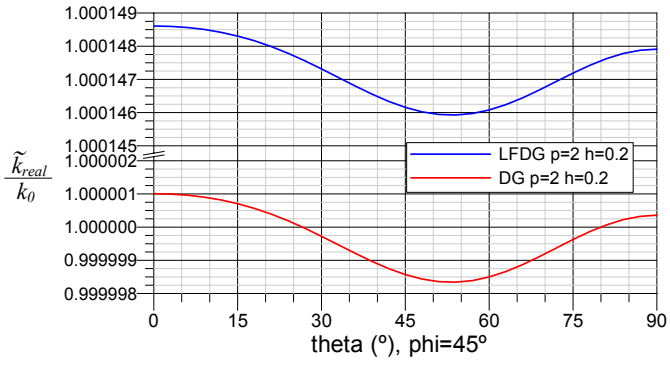

Fig. 8. Cuts of the dispersion error comparing the DG operator and the LFDG algorithm for order $p = 2$ and $h = 0.2$. The Y axes have been broken in all cases, maintaining the same spacing, in order to show the offset in the dispersion error.

(heuristically taken into account for the additional LFDG terms). This simple estimation is based on the fact that FDTD can be seen as a kind of FVTD method, which in turn is equivalent to a $p = 0$ LFDG, where the elements are cubes instead of tetrahedrons [26] (we will not consider here specific architecture-based computer-optimized FDTD codes that might render $K < 1$).

The CC magnitude has been computed for the results of the convergence analysis of Fig. 3, and shown in Fig. 9, where CC is on the X-axis and accuracy is on the Y-axis on the upper side of the plot and the resolution of the mesh, h, on the lower side.

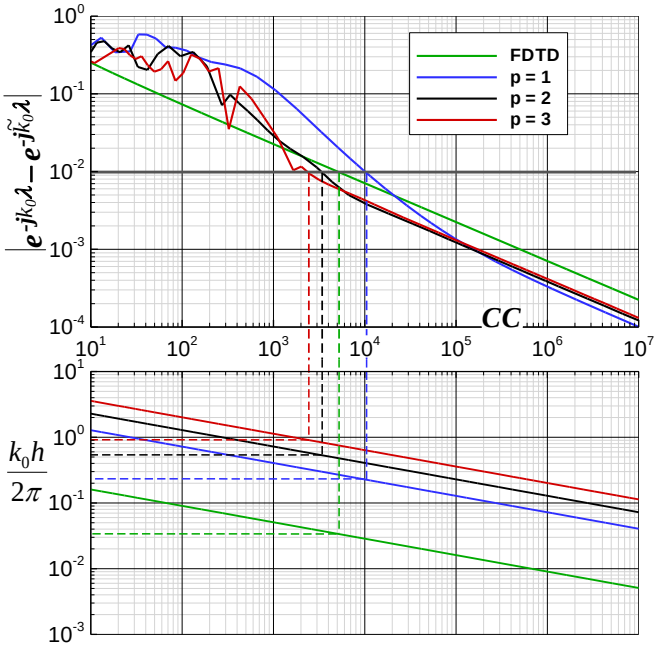

Fig. 9. Computational cost of the LFDG algorithm for $\tau = 0.1$, $\Delta t = 0.7\Delta t_{max}$ and different order of the basis functions p. CC is on the X-axis and, accuracy is on the Y-axis, on the upper side of the plot, and the resolution of the mesh, h, on the lower side. A similar curve of the FDTD method has been included for comparison.

The numerical values of CC for the 10^{-2} accuracy case appear in Table I. As expected, for higher orders p, the number of elements per wavelength $\left(\frac{\lambda}{h}\right)$ to reach this accuracy can be decreased and larger Δt are allowable. Thus, the overall computational cost decreases with higher order p. However, if we require higher accuracies ($> 10^{-3}$), this is no longer true, as seen in Fig. 9, because the global error is dominated by the 2^{nd}-order temporal integration method, and the super-convergence behavior is lost. The same reasoning explains that the gain for using $p = 3$ instead of $p = 2$ is not as high as the gain from $p = 1$ to $p = 2$. The convergence of the dispersion error for order $p = 4$ of the spatial discretization is 10, since the convergence of the simple LF is just 2, going to higher orders in the spatial discretization is not efficient. For all these reasons, we conclude that orders $p > 3$ are not efficient in practical problems in the LFDG algorithm. This is a major limitation of the method, which prevents us from taking full advantage of p refinement techniques. On the

other hand, the method has a comparable computational cost to FDTD for practical applications (from the plane-wave analysis standpoint), but preserving most of the advantages of finite-element methods (e.g. the conformal meshing or h-refinement in regions with strong spatial variations of the fields, where time integration errors are negligible).

TABLE I
RESULTS OF THE COMPUTATIONAL COST ANALYSIS FOR AN ACCURACY OF 10^{-2} PER WAVELENGTH.

	Q	$\frac{\lambda}{h}$	$\frac{M}{\lambda^3}$	$\frac{MQ(^1)}{\lambda^3}$	$c\,\Delta t\,10^3$	CC	Gain (^{2})
FDTD	3	28.5	23149	69447	14.1	4430	–
$p=1$	12	4.5	2187	26244	17.6	9660	–
$p=2$	30	1.9	165	4950	85.3	3270	2.95
$p=3$	60	1.1	32	1920	97.1	2260	1.45

(^{1}) MQ is the number of basis functions. The number of *DoF* will be $2MQ$
(^{2}) The gain has been defined as $\left(\frac{CC(p-1)}{CC(p)}\right)$

We can summarize the results given in Fig. 9 and Table I as:

- The computational cost of the LFDG method is of the same order of magnitude as the traditional FDTD method. Therefore, it is expected that LFDG has all the advantages of finite-element methods as a similar computational cost of the FDTD method.
- Due to the limitations of using a 2^{nd}-order accurate time integration scheme, it will not be worthwhile to use basis functions of order p higher that 3.
- LFDG method is an efficient algorithm for an accuracy of 10^{-2} to 10^{-3} global error per wavelength[5]. For higher accuracies, higher-order time integration methods are required to take greater advantage of the super-convergence property of the DG operator.

VII. CONCLUSIONS

In this paper, we have used a semi-analytical eigenvalue analysis to study the convergence of the DG semi-discrete scheme and compared it with the fully discrete LFDG method.

We have shown that the semi-discrete DG method with penalized flux exhibits a super-convergence behavior, with a dissipative error increasing with the basis order p more rapidly than the dispersive one. When it is combined with a 2^{nd} order LF time integration scheme (LFDG), dispersion is added (not dissipation) and corruption of the super-convergence behavior occurs. The anisotropy of the semi-discrete DG and the LFDG scheme has also been analyzed. A numerical plane-wave propagation experiment has been employed to corroborate the results found with the eigenvalue approach and illustrate the appearance of other numerical artifacts.

The accuracy limits and computational cost of the LFDG method have been explored, providing efficient criteria to tune the simulation parameters. We have shown that, for the typical accuracies required in practical problems, the LFDG method is efficient for orders $p \leq 3$. Higher accuracies could be achieved for $p > 3$ if combined with higher-order time-integration methods. We have also seen that, even for simple plane-wave propagation, the computational costs of the LFDG method are in the same order of magnitude of the traditional FDTD method, with a similar accuracy. This makes of LFDG an especially attractive alternative to FDTD for realistic problems because of its superior accuracy when dealing with curved objects and the adaptability of the unstructured meshes.

[5]In case of FDTD, for an accuracy of 10^{-2} we need a 30 samples per wavelegnth and 100 for 10^{-3}.

REFERENCES

[1] K. S. Yee, "Numerical solution of initial boundary value problems involving Maxwell's equations in isotropic media," *IEEE Transactions on Antennas and Propagation*, vol. Ap14, no. 3, pp. 302–307, 1966.

[2] A. Taflove, *Computational Electrodynamics: The Finite-Difference Time-Domain Method.* Boston: Artech House, 1995.

[3] F. Q. Hu and H. L. Atkins, "Eigensolution analysis of the discontinuous Galerkin method with nonuniform grids," *Journal of Computational Physics*, vol. 182, no. 2, pp. 516–545, November 2002.

[4] M. Ainsworth, "Dispersive and dissipative behaviour of high order discontinuous Galerkin finite element methods," *Journal of Computational Physics*, vol. 198, pp. 106–130, 2004.

[5] M. Ainsworth, P. Monk, and W. Muniz, "Dispersive and dissipative properties of discontinuous Galerkin finite element methods for the second-order wave equation," *Journal of Scientific Computing*, vol. 27, no. 1–3, pp. 3205–3223, June 2006.

[6] G. Cohen, X. Ferrieres, and S. Pernet, "A spatial high-order hexahedral discontinuous Galerkin method to solve Maxwell's equations in time domain," *Journal of Computational Physics*, vol. 217, pp. 340–363, 2006.

[7] M. H. Chen, B. Cockburn, and F. Reitich, "High-order RKDG methods for computational electromagnetics," *Journal of Scientific Computing*, vol. 22-23, pp. 205–226, June 2005.

[8] F. Q. Hu, M. Y. Hussaini, and P. Rasetarinera, "An analysis of the discontinuous Galerkin method for wave propagation problems," *Journal of Computational Physics*, vol. 151, no. 2, pp. 921–946, May 1999.

[9] D. Sármány, M. A. Botchev, and J. J. W. van der Vegt, "Dispersion and dissipation error in high-order Runge-Kutta discontinuous Galerkin discretisations of the Maxwell equations," *Scientific Computing*, vol. 33, no. 1, pp. 47–74, October 2007.

[10] J. P. Webb and S. McFee, "The use of hierarchal triangles in finite-element analysis of microwave and optical devices," *IEEE Transactions on Magnetics*, vol. 27, no. 5, pp. 4040–4043, September 1991.

[11] J. P. Webb, "Hierarchal vector basis functions of arbitrary order for triangular and tetrahedral finite elements," *IEEE Transactions on Antennas and Propagation*, vol. 47, no. 8, pp. 1244–1253, August 1999.

[12] S. D. Gedney, C. Luo, B. Guernsey, J. A. Roden, R. Crawford, and J. A. Miller, "The discontinuous Galerkin finite element time domain method (DGFETD): A high order, globally-explicit method for parallel computation," *2007 IEEE International Symposium on Electromagnetic Compatibility*, pp. 1–3, July 2007.

[13] J. Alvarez, L. D. Angulo, A. R. Bretones, and S. G. Garcia, "3D discontinuous Galerkin time domain method for anisotropic materials," *IEEE Antennas and Wireless Propagation Letters*, vol. 11, pp. 1182–1185, December 2012.

[14] J. S. Hesthaven and T. Warburton, "High-order nodal discontinuous Galerkin methods for the Maxwell eigenvalue problem," *Philosophical Transactions: Mathematical, Physical and Engineering Sciences*, vol. 362, no. 1816, pp. 493–524, March 2004.

[15] ——, *Nodal Discontinuous Galerkin Methods. Algorithms, Analysis, and Applications.* Springer Science+Business Media, LLC, 233 Spring Street, New York, NY 10013, USA: Springer, 2008.

[16] E. Montseny, S. Pernet, X. Ferriéres, and G. Cohen, "Dissipative terms and local time-stepping improvements in a spatial high order discontinuous Galerkin scheme for the time-domain Maxwell's equations," *Journal of Computational Physics*, vol. 227, pp. 6795–6820, 2008.

[17] R. Diehl, K. Busch, and J. Niegemann, "Comparison of low-storage Runge-Kutta schemes for discontinuous Galerkin time-domain simulations of Maxwell's equations," *Journal of Computational and Theoretical Nanoscience*, vol. 7, pp. 1–9, 2010.

[18] J. Alvarez, L. D. Angulo, A. R. Bretones, and S. G. Garcia, "A spurious–free Discontinuous Galerkin Time–Domain method for the accurate modeling of microwave filters," *IEEE Transactions on Microwave Theory and Techniques*, vol. 60, no. 6, pp. 2359–2369, 2012.

[19] ——, "A leap-frog discontinuous Galerkin time-domain method for HIRF assessment," *IEEE Transactions on Electromagnetic Compatibilbity*, vol. (To appear. Available as Early Access in IEEEXplore), 2013.
[20] J. Alvarez, L. D. Angulo, M. F. Pantoja, A. R. Bretones, and S. G. Garcia, "Source and boundary implementation in vector and scalar DGTD," *IEEE Transactions on Antennas and Propagation*, vol. 58, no. 6, pp. 1997–2003, 2010.
[21] J. Alvarez, L. D. Angulo, A. R. Bretones, C. M. de Jong, and S. G. Garcia, "An efficient local time?stepping DGTD method: application to antenna modeling," *IEEE Transactions on Antennas and Propagation*, (submitted).
[22] L. Fezoui, S. Lanteri, S. Lohrengel, and S. Piperno, "Convergence and stability of a discontinuous Galerkin time-domain method for the 3D heterogeneous Maxwell equations on unstructured meshes," *ESAIM: Mathematical Modelling and Numerical Analysis*, vol. 39, no. 6, pp. 1149–1176, June 2005.
[23] G. Cohen and M. Duruflé, "Non spurious spectral-like element methods for Maxwell's equations," *Journal of Computational Mathematics*, vol. 25, no. 3, pp. 282–304, 2007.
[24] J. L. Mead and R. A. Renauty, "Optimal Runge-Kutta methods for first order pseudospectral operators," *Journal of Computational Physics*, vol. 152, pp. 404–419, 1999.
[25] H. Fahs and S. Lanteri, "A high-order non-conforming discontinuous Galerkin method for time-domain electromagnetics," *Journal of Computational and Applied Mathematics*, vol. 234, pp. 1088–1096, 2010.
[26] S. G. Garcia, M. F. Pantoja, C. M. de Jong van Coevorden, A. R. Bretones, and R. G. Martin, "A new hybrid DGTD/FDTD method in 2-D," *IEEE Microwave and Wireless Components Letters*, vol. 18, no. 12, pp. 764–766, December 08.